Check for updates
Natural Product Sciences
31(2) : 129-137 (2025)
https://doi.org/10.20307/nps.2025.31.2.129

In vitro and *in silico* Analysis of PTP1B and α-Glucosidase Inhibitory Activities of Isoflavonoids Isolated from *Belamcanda chinensis* Roots

Manh Tuan Ha[1,2], Thi Thanh Le[1], Trong Trieu Tran[1], Thu Huong Tran[3], Jeong Ah Kim[4,*], and Byung Sun Min[1,*]

[1]*College of Pharmacy, Drug Research and Development Center, Daegu Catholic University, Gyeongbuk 38430, Republic of Korea*
[2]*College of Pharmacy, Thanh Do University, Hanoi, Vietnam*
[3]*School of Chemistry and Life Sciences, Hanoi University of Science and Technology Hanoi, Vietnam*
[4]*College of Pharmacy, Research Institute of Pharmaceutical Sciences, Kyungpook National University, Daegu 41566, Republic of Korea*

Abstract – Type 2 diabetes (T2D) is currently the most prevalent form of diabetes and an expanding global health problem. α-Glucosidase and protein tyrosine phosphatase 1B (PTP1B) are well-known as the promising target enzymes for the treatment of T2D. In our continuing search for new antidiabetic substances from Korean medicinal plants, twelve isoflavonoids and four flavonoids were isolated and structurally determined from the roots of *Belamcanda chinensis,* and their α-glucosidase and PTP1B inhibitory activities were investigated *in vivo* and *in silico*. The results showed that two isoflavonoids (irilin D and genistein) act as dual α-glucosidase and PTP1B inhibitors: moderately inhibited PTP1B [irilin D (IC_{50} = 31.86 μM) and genistein (IC_{50} = 24.64 μM)] and significantly inhibited α-glucosidase [irilin D (IC_{50} = 44.22 μM) and genistein (IC_{50} = 14.71 μM)] in comparison to the positive controls, ursolic acid (IC_{50} = 5.99 μM) and acarbose (IC_{50} = 216.30 μM), respectively. To the best of our knowledge, this is the first investigation on the inhibitory activity of irilin D against PTP1B and α-glucosidase enzymes. The kinetic investigation of irilin D indicated its noncompetitive inhibition type for both of these two enzymes. In addition, molecular docking results showed that irilin D exhibited good binding affinities toward both PTP1B and α-glucosidase with negative binding energies. The results suggested the potential of *B. chinensis* isoflavonoids in the prevention and treatment of T2D.
Keywords – *Belamcanda chinensis,* Iridaceae, Isoflavonoids, PTP1B, α-Glucosidase, Molecular docking

Introduction

Type 2 diabetes (T2D), also known as non-insulin-dependent diabetes mellitus, is currently the most prevalent form of diabetes and the number of people affected by this pathology is continuously increasing worldwide. The International Diabetes Federation (IDF) estimates that 536.6 million people are living with diabetes (diagnosed or undiagnosed) in 2021, and this number is projected to increase by 46%, reaching 783.2 million by 2045.[1] T2D is characterized by insulin resistance—possibly due to diminished post-receptor insulin signaling. T2D is characterized by insulin resistance—possibly due to diminished post-receptor insulin signaling, which typically begins several years before hyperglycemia.[2] α-Glucosidase and protein tyrosine phosphatase 1B (PTP1B) are well-known as the promising target enzymes for the treatment of T2D.[3] α-Glucosidase is an enzyme that catalyzes glucose release from the nonreducing end of dietary carbohydrates, thereby elevating the blood glucose level. Therefore, inhibition of α-glucosidase is one of the well-established therapeutic approaches for controlling postprandial hyperglycemia.[3] While protein tyrosine phosphatase 1B (PTP1B) plays an important role in the negative regulation of insulin signal transduction pathway and has been validated as a novel therapeutic strategy for the treatment of type 2 diabetes. Inhibition of PTP1B can improve insulin sensitivity, suggesting that the PTP1B inhibitors are conducive to T2D treatment.[4] It has been recognized that natural phytochemicals with dual inhibition of α-glucosidase and PTP1B enzymes effectively suppress hyperglycemia due to their synergistic effect and significantly contribute to

*Corresponding Authors
Jeong Ah Kim, Ph.D., College of Pharmacy, Research Institute of Pharmaceutical Sciences, Kyungpook National University, Daegu 41566, Republic of Korea
Tel: +82-53-950-8574; E-mail: jkim6923@knu.ac.kr

Byung Sun Min, Ph.D., College of Pharmacy, Drug Research and Development Center, Daegu Catholic University, Gyeongbuk 38430, Republic of Korea
Tel: +82-53-850-3613; E-mail: bsmin@cu.ac.kr

the enhancement of insulin sensitivity.[3,5]

Belamcanda chinensis (L.) DC (syn. *Iris domestica* and known as "sa kan" in Korea) belongs to the Iridaceae family and is widely distributed in East and Southeast Asia and North America.[6] With pharmacological effects such as reducing throat swelling, clearing heat, and detoxifying, this plant is used in traditional medicines to treat sore throat, cough, bronchitis, and chronic tracheitis.[7,8] Previous phytochemical investigations on *B. chinensis* reported iridal-type triterpenoids, isoflavonoids, flavonoids, benzoquinones, and steroids.[6–10] Various pharmacological activities have been reported from the components and extracts of *B. chinensis* such as anti-osteoclastogenic, anti-inflammatory, antidiabetic, antioxidant, antitumor, hepatoprotective, antimutagenic, neuroprotective, antibacterial, and neuroprotective activities.[6-10] In our previous study, six sucrosephenylpropanoid esters, five iridal-type triterpenoids, twelve isoflavonoids, and four flavonoids were isolated from *B. chinensis* roots.[10] Among them, one sucrosephenylpropanoid ester (belamchinoside A) and one isoflavonoid (irilin D) exhibited strong effects on RANKL-induced osteoclast formation using RAW 264.7 cells and BMMs in a concentration-dependent manner.[10] In this present study, we report the isolation and NMR characterization of twelve isoflavonoids and four flavonoids from the *B. chinensis* roots, as well as the investigation of their inhibitory ability against α-glucosidase and PTP1B enzymes *in vivo* and *in silico*.

Experimental

Chemicals and reagents – Protein tyrosine phosphatase 1B (PTP1B, human recombinant) and dithiothreitol (DTT) were purchased from Biomol® International LP (Plymouth Meeting, PA, USA) and Bio-Rad Laboratories (Hercules, CA, USA), respectively. Yeast α-glucosidase, *p*-nitrophenyl phosphate (*p*-NPP), *p*-nitrophenylα-D-glucopyranoside (*p*-NPG), acarbose, ethylene diamine tetraacetic acid (EDTA), and dimethylsulfoxide (DMSO) were purchased from Sigma-Aldrich Co. (St. Louis, MO, USA).

Plant material – The plant sample (*B.chinensis* roots) was collected at the Medicinal Plants Garden of Daegu Catholic University, Republic of Korea, in May 2024, and authenticated by Professor Byung Sun Min, College of Pharmacy, Daegu Catholic University, Republic of Korea. The voucher specimen (CUD-24052) was stored at the Laboratory of Pharmacognosy in the College of Pharmacy, Daegu Catholic University, Republic of Korea.

Extraction and isolation – The dried roots (1.5 kg) of *B. chinensis* were extracted four times with methanol (MeOH, 5 L for 3 hours each) at room temperature and filtered. The filtrate was evaporated under reduced pressure to obtain the MeOH extract (305 g), which was suspended in distilled water and successively partitioned with with *n*-hexane, CH_2Cl_2, and EtOAc, respectively. The CH_2Cl_2 fraction (73 g) was separated into ten fractions (MC1-MC10) using column chromatography (CC), silica gel (CH_2Cl_2:MeOH; 50:1 → 0:1, v/v). Fraction MC7 (11 g) was subjected to silica gel column chromatography (CC) and eluted with a solvent system of *n*-hexane-acetone (5:1, v/v) to yield compounds **2** (0.8 g) and **1** (135 mg). Fraction MC6 (358 mg) was chromatographed on a Sephadex LH-20 column (MeOH-H_2O, 2:1, v/v) to yield compounds **3** (6 mg) and **4** (5 mg). Fraction MC5 (326 mg) was further purified using an RP-18 silica gel column (MeOH-H_2O, 2:1, v/v) to yield compounds **6** (6 mg) and **5** (4 mg). Fraction MC8 (5.2 g) was separated using an RP-18 silica gel column (MeOH-H_2O, 2:1, v/v) to yield seven sub-fractions (MC8.1–MC8.7). Sub-fractions MC8.3 (216 mg) was subjected to Sephadex LH-20 CC (MeOH-H_2O, 1.5:1, v/v) to yield compound **7** (5 mg). The EtOAc fraction (34 g) was chromatographed on a silica gel column (CH_2Cl_2-MeOH, 15:1 to 0:1, v/v) to yield five fractions (E1–E5). Fraction E1 (4 g) was separated using a silica gel column (*n*-hexane-CH_2Cl_2-MeOH, 3:5:0.3, v/v/v) to give compounds **9** (5 mg) and **12** (7 mg). Fraction E2 (209 mg) was purified using a Sephadex LH-20 CC eluted with a mixture of MeOH-H_2O (2:1, v/v) to give **10** (6 mg). Fraction E3 (3.9 g) was subjected to a silica gel column (CH_2Cl_2-MeOH, 30:1, v/v) to give compounds **11** (5 mg) and **8** (7 mg). Fraction E4 (5.6 g) was chromatographed on a silica gel column (CH_2Cl_2-MeOH, 20:1, v/v) to yield four fractions (E4.1-E4.4). Compounds **16** (5.5 mg) and **15** (7 mg) were isolated from subfraction E4.3 (358 mg) by RP-18 silica gel CC (MeOH-H_2O, 2:1, v/v). Fraction E5 (368 mg) was purified using a RP-18 silica gel column (MeOH-H_2O, 3:1, v/v). to yield compounds **13** (7 mg) and **14** (5 mg).

3,5,4'-trihydroxy-7,5'-dimethoxyflavanone (5) – Yellow amorphous powder; ^{1}H-NMR (400 MHz, methanol-d_4): δ 7.14 (1H, d, J = 2.0 Hz, H-6′), 7.01 (1H, dd, J = 8.0, 2.0 Hz, H-2′), 6.87 (1H, d, J = 8.0 Hz, H-3′), 6.11 (1H, s, H-8), 6.08 (1H, s, H-6), 5.05 (1H, d, J = 11.2 Hz, H-2), 4.64 (1H, d, J = 11.2 Hz, H-3), 3.91 (3H, s, -OCH_3-7), 3.84 (3H, s, -OCH_3-5′); ^{13}C-NMR (100 MHz, methanol-d_4) δ (ppm): 198.9 (C-4), 169.8 (C-7), 165.0 (C-5), 164.3 (C-8a), 148.9 (C-4′), 148.4 (C-5′), 129.7 (C-1′), 122.2 (C-2′), 115.9 (C-3′), 112.5 (C-6′), 102.6 (C-4a), 96.0 (C-6), 95.1 (C-8), 85.3 (C-2), 73.7 (C-3), 56.5 (-OCH_3-5′), 56.4 (-OCH_3-7).

3,5,3'-trihydroxy-7,4',5'-trimethoxyflavanone (6) – Yellow amorphous powder; ^{1}H-NMR (400 MHz, methanol-

d_4): δ 6.74 (1H, s, H-6′), 6.73 (1H, s, H-2′), 6.13 (1H, s, H-8), 6.11 (1H, s, H-6), 5.03 (1H, d, J = 11.2 Hz, H-2), 4.60 (1H, d, J = 11.2 Hz, H-3), 3.90 (3H, s, -OCH_3-5′), 3.86 (3H, s, -OCH_3-7), 3.85 (3H, s, -OCH_3-4′); ^{13}C-NMR (100 MHz, methanol-d_4): 198.7 (C-4), 169.8 (C-7), 165.0 (C-5), 164.7 (C-8a), 154.5 (C-3′), 151.1 (C-5′), 138.1 (C-4′), 134.1 (C-1′), 109.9 (C-2′), 104.5 (C-6′), 102.6 (C-4a), 96.1 (C-6), 95.1 (C-8), 85.2 (C-2), 73.7 (C-3), 60.9 (-OCH_3-5′), 56.5 (-OCH_3-7), 56.4 (-OCH_3-4′).

Noririsflorentin (7) – Yellow amorphous powder; ^{1}H-NMR (400 MHz, methanol-d_4): δ 8.05 (1H, s, H-2), 6.79 (2H, s, H-2′ and 6′), 6.73 (1H, s, H-8), 6.10 (2H, s, H-9), 4.05 (3H, s, -OCH_3-4′), 3.87 (6H, s, -OCH_3-3′ and 5′); ^{13}C-NMR (100 MHz, methanol-d_4), see Table 1.

Irilin D (8) – Yellow amorphous powder; ^{1}H-NMR (400 MHz, acetone-d_6): δ 13.2 (1H, s, OH-5), 8.13 (1H, s, H-2), 7.14 (1H, d, J = 2.0 Hz, H-6′), 6.94 (1H, dd, J = 8.0, 2.0 Hz, H-2′), 6.88 (1H, d, J = 8.0 Hz, H-3′), 6.47 (1H, s, H-8), 3.86 (3H, s, -OCH_3-6); ^{13}C-NMR (100 MHz, methanol-d_4), see Table 1.

Dichotomitin (9) – Yellow amorphous powder; ^{1}H-NMR (400 MHz, methanol-d_4): δ 8.47 (1H, s, H-2), 6.87 (1H, s, H-8), 6.72 (1H, s, H-2′), 6.67 (1H, s, H-6′), 6.17 (2H, s, H-9), 3.79 (3H, s, -OCH_3-5′), 3.69 (3H, s, -OCH_3-4′); ^{13}C-NMR (100 MHz, methanol-d_4), see Table 1.

Genistein (10) – Yellow amorphous powder; ^{1}H-NMR (400 MHz, methanol-d_4): δ 8.06 (1H, s, H-2), 7.39 (2H, d, J = 8.0 Hz, H-2′ and 6′), 6.87 (2H, d, J = 8.0 Hz, H-3′ and 5′), 6.35 (1H, s, H-8), 6.23 (1H, s, H-6); ^{13}C-NMR (100 MHz, methanol-d_4), see Table 1.

Hispidulin (11) – Yellow amorphous powder; ^{1}H-NMR (400 MHz, DMSO-d_6): δ 7.92 (2H, d, J = 8.8 Hz, H-2′, 6′), 6.92 (2H, d, J = 8.8 Hz, H-3′, 5′), 6.76 (1H, s, H-3), 6.58 (1H, s, H-8), 3.74 (3H, s, -OCH_3-6); ^{13}C-NMR (100 MHz, DMSO-d_6): δ 182.1 (C-4), 163.8 (C-4′), 161.2 (C-2), 157.4 (C-7), 152.8 (C-5), 152.4 (C-8a), 131.4 (C-6), 128.5 (C-2′ and 6′), 121.2 (C-1′), 116.0 (C-3′ and 5′), 104.1 (C-4a), 102.4 (C-3), 94.3 (C-8), 60.0 (-OCH_3-6).

Kanzakiflavone-2 (12) – Yellow amorphous powder; ^{1}H-NMR (400 MHz, DMSO-d_6): δ 7.94 (2H, d, J = 8.4 Hz, H-2′ and 6′), 6.94 (2H, d, J = 8.4 Hz, H-3′ and 5′), 6.91 (1H, s, H-3), 6.85 (1H, s, H-8), 6.16 (2H, s, -OCH_2O-9); ^{13}C-NMR (100 MHz, DMSO-d_6): δ 182.5 (C-4), 164.1 (C-4′), 161.3 (C-2), 153.7 (C-7), 152.5 (C-8a), 141.1 (C-5), 129.4

Table 1. ^{13}C-NMR data of isoflavonoids **1**–**4** and **7**–**10**

Position	**1** [a]	**2** [a]	**3** [b]	**4** [b]	**7** [b]	**8** [c]	**9** [b]	**10** [b]
2	153.3	153.8	155.1	155.1	153.2	154.5	155.2	154.8
3	121.7	124.1	124.0	123.0	123.7	123.5	122.1	123.3
4	180.3	173.7	182.5	182.9	177.5	182.0	180.6	182.2
4a	104.8	113.1	106.7	109.2	114.0	106.5	107.4	106.2
5	152.9	140.5	154.9	155.1	155.0	154.5	141.5	163.8
6	131.4	135.9	132.8	143.3	142.4	132.1	129.7	100.1
7	157.5	152.6	158.7	155.9	156.3	157.8	154.0	165.9
8	93.9	93.6	94.9	90.3	93.9	94.3	89.5	94.7
8a	152.6	152.0	154.6	155.1	149.0	154.1	152.9	159.7
9		102.6		104.3	103.9		102.9	
1′	126.1	127.5	125.1	124.6	126.7	123.6	125.8	124.7
2′	110.4	106.7	121.5	131.4	107.9	121.5	110.4	131.3
3′	150.2	152.5	112.6	116.3	153.2	115.9	152.9	116.2
4′	136.4	137.3	149.2	158.9	136.5	146.2	136.4	158.8
5′	154.8	152.5	147.4	116.3	153.2	145.6	150.3	116.2
6′	104.6	106.7	117.3	131.4	107.9	117.2	104.5	131.3
3′-OMe		55.9			56.8			
4′-OMe	59.9	60.0	56.4		61.2		59.9	
5′-OMe	55.8	55.9			56.8		55.8	
5-OMe		60.7						
6-OMe	59.9		60.9			60.6		

^{13}C NMR were measured in DMSO-d_6 [a], methanol-d_4 [b], acetone-d_6 [c]

(C-6), 128.5 (C-2′ and 6′), 120.9 (C-1′), 116.0 (C-3′ and 5′), 106.6 (C-4a), 102.7 (C-3), 102.7 (-OCH_2O-9), 89.7 (C-8).

Tectoridin (13) – Yellow amorphous powder; ^{1}H-NMR (400 MHz, DMSO-d_6): δ 8.37 (1H, s, H-2), 7.34 (2H, d, J = 8.4 Hz, H-2′ and 6′), 6.77 (2H, d, J = 8.4 Hz, H-3′ and 5′), 6.82 (1H, s, H-8), 3.70 (3H, s, -OCH_3-6), 5.05 (1H, d, J = 7.2 Hz, H-1″), 3.65, 3.42 (each 1H, m, H_2-6″), 3.58 (1H, m, H-3″), 3.42 (1H, m, H-5″), 3.26 (1H, m, H-2″), 3.14 (1H, m, H-4″); ^{13}C NMR (100 MHz, DMSO-d_6): δ 180.8 (C-4), 157.5 (C-4′), 156.6 (C-7), 154.7 (C-2), 152.9 (C-5), 152.5 (C-8a), 132.4 (C-6), 130.2 (C-2′ and 6′), 122.1 (C-1′), 121.1 (C-3), 115.1 (C-3′ and 5′), 106.5 (C-4a), 100.1 (C-1″), 94.0 (C-8), 77.3 (C-5″), 76.7 (C-3″), 73.1 (C-2″), 69.7 (C-4″), 60.7 (CH_2-6″), 60.3 (-OCH_3-6).

Iridin (14) – Yellow amorphous powder; ^{1}H-NMR (400 MHz, acetone-d_6): δ 8.29 (1H, s, H-2), 6.79 (1H, d, J = 2.0 Hz, H-2′), 6.78 (1H, d, J = 2.0 Hz, H-6′), 6.85 (1H, s, H-8), 3.85 (3H, s, -OCH_3-5′), 3.81 (3H, s, -OCH_3-6), 3.78 (3H, s, -OCH_3-4′), 5.18 (1H, d, J = 7.2 Hz, H-1″), 3.43–3.92 (sugar protons); ^{13}C-NMR (100 MHz, acetone-d_6): 181.8 (C-4), 157.9 (C-7), 155.6 (C-5), 154.7 (C-8a), 153.8 (C-2), 153.7 (C-5′), 151.1 (C-3′), 137.4 (C-4′), 134.4 (C-6), 127.4 (C-1′), 123.7 (C-3), 110.6 (C-2′), 107.9 (C-4a), 105.8 (C-6′), 101.6 (C-1″), 95.0 (C-8), 78.1 (C-5″), 78.0 (C-3″), 74.5 (C-2″), 71.7 (C-4″), 62.5 (CH_2-6″), 60.8 (-OCH_3-4′), 60.7 (-OCH_3-6), 56.3 (3H, s, -OCH_3-5′).

6″-*O*-*p*-hydroxybenzoyliridin (15) – Yellow amorphous powder; ^{1}H-NMR (400 MHz, acetone-d_6): δ 8.17 (1H, s, H-2), 7.94 (2H, d, J = 8.8 Hz, H-2‴ and 6‴), 6.94 (2H, d, J = 8.4 Hz, H-3‴ and 5‴), 6.84 (1H, s, H-8), 6.80 (1H, d, J = 2.0 Hz, H-2′), 6.80 (1H, d, J = 2.0 Hz, H-6′), 5.27 (1H, d, J = 7.2 Hz, H-1″), 4.76 (1H, dd, J = 12.0, 2.0 Hz, H-6″a), 4.38 (1H, dd, J = 12.0, 8.0 Hz, H-6″b), 4.04 (1H, m, H-5″), 3.88 (3H, s, -OCH_3-5′), 3.82 (3H, s, -OCH_3-4′), 3.81 (3H, s, -OCH_3-6), 3.67 (1H, m, H-3″), 3.66 (1H, m, H-2″), 3.53 (1H, m, H-4″); ^{13}C-NMR (100 MHz, acetone-d_6): δ 181.8 (C-4), 166.3 (C-7‴), 162.7 (C-4‴), 157.7 (C-7), 155.2 (C-2), 154.8 (C-5), 153.9 (C-5′), 153.6 (C-8a), 151.0 (C-3′), 137.4 (C-4′), 134.1 (C-6), 132.6 (C-2‴ and 6‴), 127.4 (C-1′), 123.7 (C-1‴), 122.3 (C-3), 116.0 (C-3‴ and 5‴), 110.7 (C-2′), 108.0 (C-4a), 105.9 (C-6′), 101.4 (C-1″), 94.9 (C-8), 77.9 (C-5″), 75.3 (C-3″), 74.4 (C-2″), 71.5 (C-4″), 64.6 (CH_2-6″), 60.8 (-OCH_3-4′), 60.7 (-OCH_3-6), 56.3 (3H, s, -OCH_3-5′).

6″-*O*-vanilloyliridin (16) – Yellow amorphous powder; ^{1}H-NMR (400 MHz, methanol-d_4): δ 7.83 (1H, s, H-2), 7.53 (1H, dd, J = 8.4, 2.0 Hz, H-6‴), 7.47 (1H, d, J = 2.0 Hz, H-2‴), 6.78 (1H, d, J = 8.4 Hz, H-5‴), 6.70 (2H, s, H-2′ and 6′), 6.57 (1H, s, H-8), 5.08 (1H, d, J = 7.2 Hz, H-1″), 4.66 (1H, dd, J = 12.0, 2.0 Hz, H-6″a), 4.45 (1H, dd, J = 12.0, 8.0 Hz, H-6″b), 3.87 (3H, s, -OCH_3-5′), 3.83 (3H, s, -OCH_3-4′), 3.79 (3H, s, -OCH_3-6), 3.77 (3H, s, -OCH_3-3‴), 3.37–3.62 (4H, m, H-2″, 3″, 4″ and 5″); ^{13}C-NMR (100 MHz, methanol-d_4): δ 182.3 (C-4), 166.7 (C-7‴),

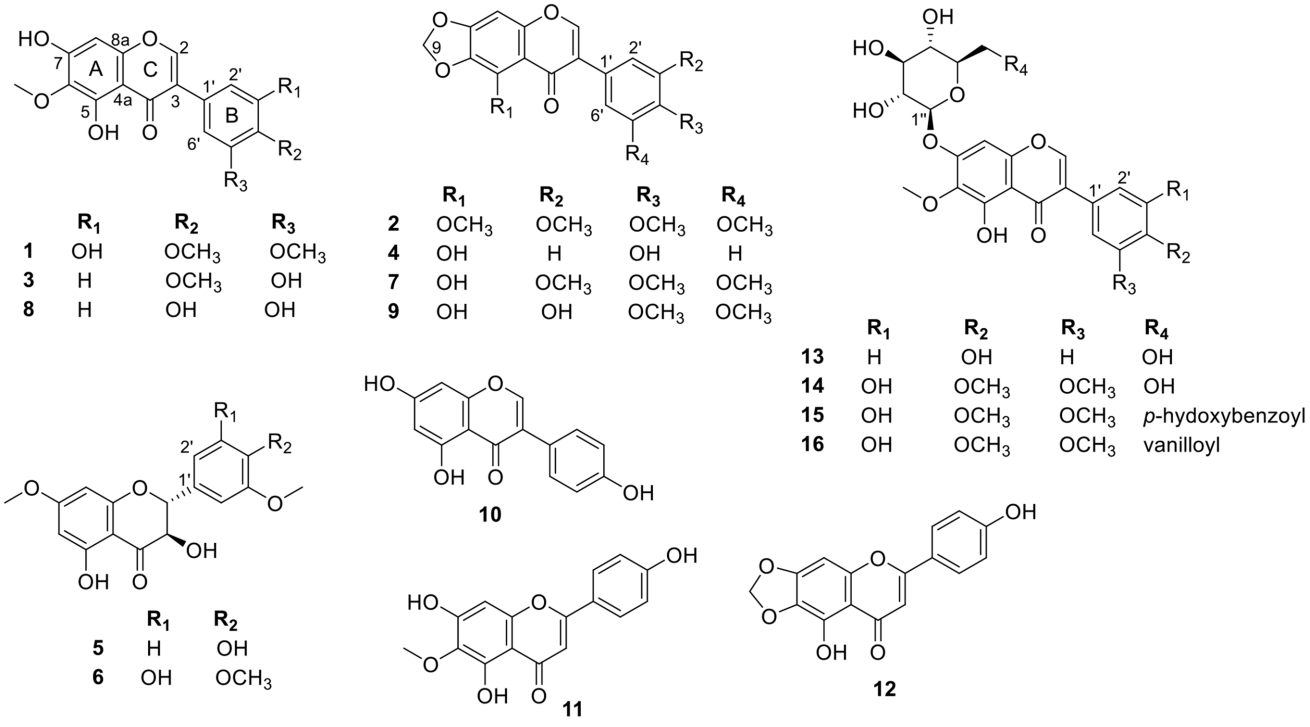

Fig. 1. Chemical structures of compounds **1**–**16**

152.8 (C-4‴), 157.6 (C-7), 155.7 (C-2), 154.6 (C-5), 154.5 (C-5′), 154.1 (C-8a), 151.5 (C-3′), 137.9 (C-4′), 134.1 (C-6), 122.4 (C-6‴), 115.9 (C-6‴), 127.7 (C-1′), 124.3 (C-1‴), 122.3 (C-3), 113.8 (C-2‴), 148.6 (C-3‴), 111.2 (C-2′), 108.3 (C-4a), 106.1 (C-6′), 101.4 (C-1″), 95.3 (C-8), 77.8 (C-5″), 75.8 (C-3″), 74.6 (C-2″), 72.1 (C-4″), 64.9 (CH_2-6″), 61.4 (-OCH_3-4′), 61.1 (-OCH_3-6), 56.6 (3H, s, -OCH_3-5′), 56.3 (3H, s, -OCH_3-3‴).

PTP1B and α-glucosidase inhibitory assays – The inhibition assays against recombinant human protein tyrosine phosphatase 1B and *α*-glucosidase enzymes were conducted with *p*-nitrophenyl phosphate (*p*-NPP) and *p*-nitrophenyl *α*-D-glucopyranoside (*p*-NPG) as the substrates, respectively, according to our previously published protocols.[5,11]

Enzyme kinetic analysis with PTP1B and α-glucosidase – The kinetic mechanisms of the active compound (irilin D, **8**) in PTP1B and glucosidase inhibition were investigated using complementary Lineweaver–Burk and Dixon plots.[5,11] The inhibition of irilin D (**8**) against PTP1B and *α*-glucosidase enzymes was monitored at different substrate concentrations (2, 1, and 0.5 mM of *p*-NPP for PTP1B and 2.5, 1.25, and 0.625 mM of *p*-NPG for *α*-glucosidase) on Dixon plots (single reciprocal plots). In addition, Lineweaver-Burk plots for the inhibition of PTP1B and *α*-glucosidase of irilin D (**8**) were obtained in the presence of its various concentrations (0, 21.5, 38.2, and 55.5 μM for PTP1B and 0, 32.5, 44.0, and 60.5 μM for *α*-glucosidase). The kinetic results were analyzed using the SigmaPlot 12.0 software (SPCC Inc., Chicago IL, U.S.A). The kinetic data were graphically presented by the Lineweaver-Burk and Dixon plots, from which the type of enzyme inhibition was determined. Kinetic constant values (K_i) were assessed using Dixon plots.

Molecular docking simulation in PTP1B and α-glucosidase inhibition – Molecular docking simulations of irilin D (**8**) against PTP1B and *α*-glucosidase enzymes were performed using AutoDock 4.2 software, according to our previously published protocol.[5,11] The complex structure of PTP1B (PDB ID of 1T49) and its selective allosteric inhibitor 3-(3,5-dibromo-4-hydroxy-benzoyl)-2-ethyl-benzofuran-6-sulfonic acid (4-sulfamoyl-phenyl)-amide (compound A), together with isomaltase (PDB ID: 3A4A) were obtained from the RCSB Protein Data Bank (https://www.rcsb.org/). Isomaltase, with the same organism and highly similar to α-glucosidase, was used as a substitute in this study. The 3D structure of (*Z*)-3-butylidenephthalide (BIP) was obtained from the PubChem Compound (NCBI) with compound CID of 5352899. The results were analyzed using Discovery Studio and PyMOL.

Statistical analysis – Statistical analyses were performed by one-way analysis of variance (ANOVA), followed by the Fisher least significant difference test. $p<0.05$ was considered statistically significant. The results are presented as the mean ± standard error of the mean (SEM).

Results and Discussion

The structure of isolated compounds were identified as irigenin (**1**),[12] irisflorentin (**2**),[12] iristectorigenin A (**3**),[13] irilone (**4**),[14] 3,5,4'-trihydroxy-7,5'-dimethoxyflavanone (**5**),[15] 3,5,3'-trihydroxy-7,4',5'-trimethoxyflavanone (**6**),[16] noririsflorentin (**7**),[17] irilin D (**8**),[18] dichotomitin (**9**),[19] genistein (**10**),[19] hispidulin (**11**),[20] kanzakiflavone-2 (**12**),[21] tectoridin (**13**),[19] iridin (**14**),[19] 6″-*O*-*p*-hydroxybenzoyliridin (**15**),[22] and 6″-*O*-vanilloyliridin (**16**)[22] (Fig. 1) based on the analysis of their observed and reported spectroscopic data.

The anti-diabetic potential of the *B. chinensis* compounds (**1**-**16**) was investigated via their inhibition against PTP1B and α-glucosidase, and the results are expressed as IC_{50} values (Table 2). Whereby, three isoflavonoids including irilone (**4**, IC_{50} = 37.95 μM), irilin D (**8**, IC_{50} = 31.86 μM), and genistein (**10**, IC_{50} = 24.64 μM) showed moderate inhibition against PTP1B in comparison to the positive control, ursolic acid (IC_{50} = 5.99 μM). Interestingly, these three compounds displayed potent α-glucosidase inhibitory activity with corresponding IC_{50} values of 76.92, 44.22, and 14.71 μM, significantly lower than the IC_{50} value (216.30 μM) of the positive control, acarbose. The remaining compounds showed weak or no activity. Similar structure-activity relationships were observed in PTP1B and α-glucosidase assays for the isoflavonoids **1**-**4** and **7**-**10**. The structures of these isoflavonoids are similar, except for the absence of the methoxy substituents in the B ring of active compounds irilone (**4**), irilin D (**8**), and genistein (**10**). This interesting finding suggested that the presence of the methoxy substituents in the B ring of isoflavonoids might have negatively affected the PTP1B and α-glucosidase inhibitory activities of the isoflavonoids. These results are consistent with the previous reports about the PTP1B and α-glucosidase inhibitory activities of genistein (**10**) and its derivatives.[23,24] To the best of our knowledge, this is the first investigation on the inhibitory activity of irilin D (**8**) against PTP1B and α-glucosidase enzymes. Therefore, this compound was selected for the kinetic and molecular docking studies.

To determine the PTP1B and α-glucosidase inhibition mechanisms of irilin D (**8**), two kinetic methods were used, the Lineweaver-Burk plot and Dixon plot. The inhibition mechanisms of each enzymatic inhibition at various

Table 2. Inhibitory activities of compounds **1-16** against PTP1B and α-glucosidase

Compounds	PTP1B			α-glucosidase		
	IC_{50} (μM ± SD)	Inhibition type	K_i (μM)	IC_{50} (μM ± SD)	Inhibition type	K_i (μM) [a]
4	37.95 ± 0.96			>100		
5	65.24 ± 1.74			76.92 ± 1.75		
8	31.86 ± 0.15	noncompetitive	30.83 ± 0.62	44.22 ± 0.59	noncompetitive	44.22 ± 0.98
10	24.64 ± 1.74			14.71 ± 0.12		
12	51.93 ± 1.31			> 100		
1–3, 6, 7, 9, 11, 13–16	> 100	-	-	> 100	-	-
Ursolic acid	5.99 ± 0.23	-	-	-	-	-
Acarbose	-	-	-	216.30 ± 1.46	-	-

concentrations of irilin D (**8**) were evaluated by monitoring the effects of various substrate concentrations via the Dixon plot, and the effects of various concentrations of irilin D (**8**) were evaluated via the Lineweaver-Burk plot. In the Lineweaver-Burk plot, the plotted lines for irilin D (**8**) that crossed the same point on the *x*-intercept, represented the noncompetitive inhibition of irilin D (**8**) against both PTP1B and *α*-glucosidase. The inhibition constants (K_i) were calculated by interpretation of the Dixon plots, where the value of the x-axis means - K_i. As a result, the inhibition

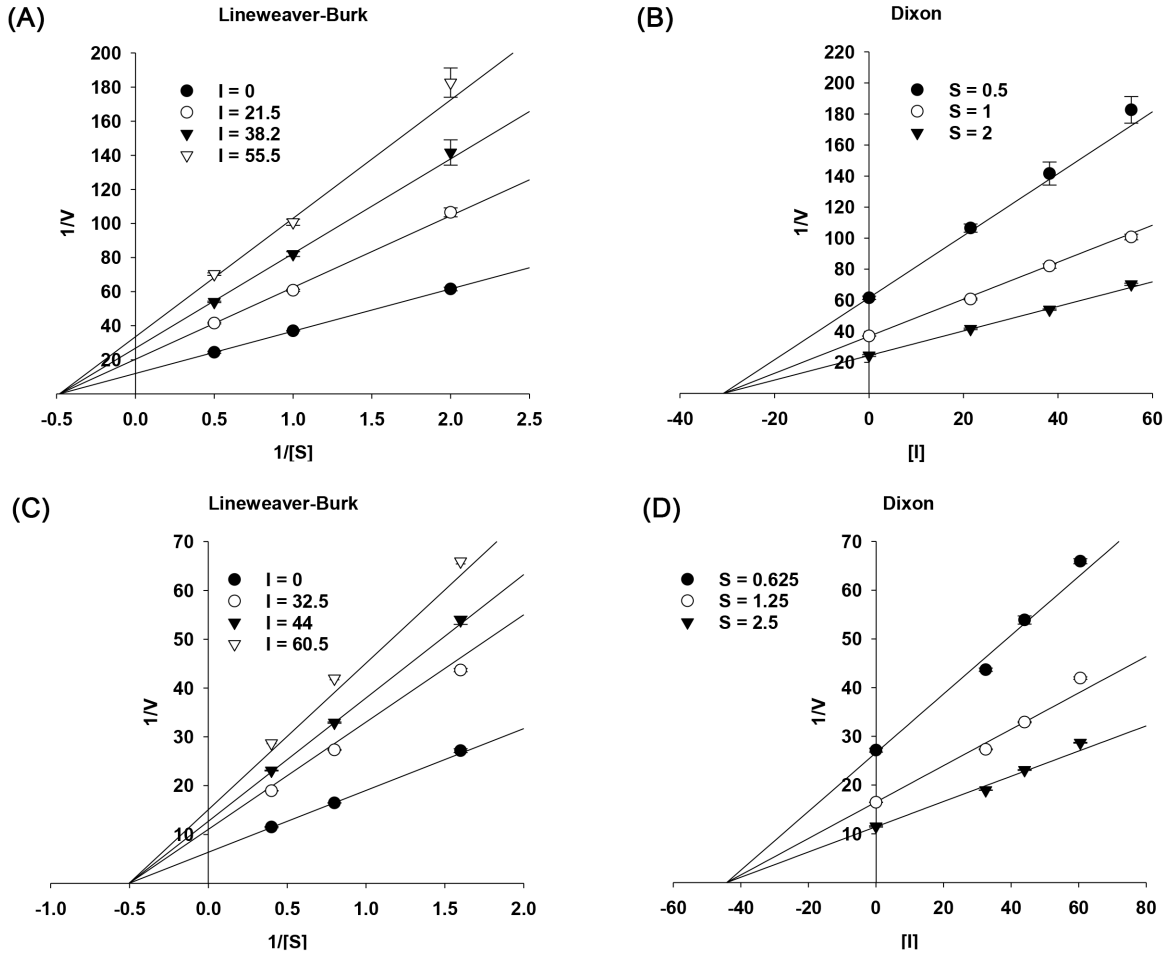

Fig. 2. Lineweaver-Burk and Dixon plots for the inhibition of PTP1B [(A) and (B)] and α-glucosidase [(C) and (D)] enzymes by irilin D (**8**), respectively.

Table 3. Binding site residues and docking scores of irilin D (**8**) and reference compounds in PTP1B and α-glucosidase

Compounds	Binding energy[c] (kcal/mol)	Hydrogen bond interaction[d] (bond distance)	van der Waals interaction[d]	Other interaction[d]
PTP1B inhibition				
8	–7.92	Asn193 (3.15 & 3.47 Å) Ala189 (3.14 Å) Lys197 (2.57 Å)	Glu276, Phe194, Glu200, Gly277	Ala189 (Alkyl), Leu192 (π-σ), Phe280 (π-π Stacked), Phe196 (π-π Stacked, Amide-π Stacked)
A[a]	–11.16	Asn193 (3.25 Å) Glu276 (4.0 Å) Phe280 (3.24 & 3.29 Å)	Pro188, Lys197, Met282, Gly277, Ile281, Glu200, Lys279	Phe196 (Amide-π Stacked, π-Alkyl), Ala189 (π-Alkyl), Phe280 (π-π Stacked), Leu192 (π-Alkyl, Alkyl)
α-glucosidase inhibition				
8	–8.23	Cys342 (3.71 Å), Glu296 (4.64 & 5.84 Å), Asn259 (3.96 & 4.29 Å)	Lys16, Thr340, Asp341, Trp343, Ser298, Thr290, Trp15, Lys13, His295, Ile272	Ala292 (π-σ)
BIP[b]	–6.86	Glu296 (4.26 Å), His295 (4.36 Å)	Asp341, Thr290, Trp343, Cys342, Asn259, Arg294, Ser291, Ser298, Lys16	Ala292 (π-σ, Alkyl), Trp15 (π-Alkyl)

[a] Reported PTP1B allosteric inhibitor. [b] Reported α-glucosidase allosteric inhibitor. [c] Estimated binding-free energy of the ligand-receptor complex. [d] All amino acid residues were located 6.0 Å from the original enzyme/inhibitor complex in the AutoDock 4.2 program.

constants of irilin D (**8**) against PTP1B and *α*-glucosidase were determined as 30.83 and 44.22 μM, respectively.

The interaction and binding modes of irilin D (**8**) with PTP1B were investigated via the simulation and comparison with the reference ligand, compound A (an allosteric inhibitor), using AutoDock 4.2 software. According to the simulation results shown in Fig. 3, both the reference ligand and irilin D (**8**) were stably positioned into the same pocket (allosteric site) of PTP1B with negative binding energies of −11.16 and −7.92 kcal/mol, respectively.

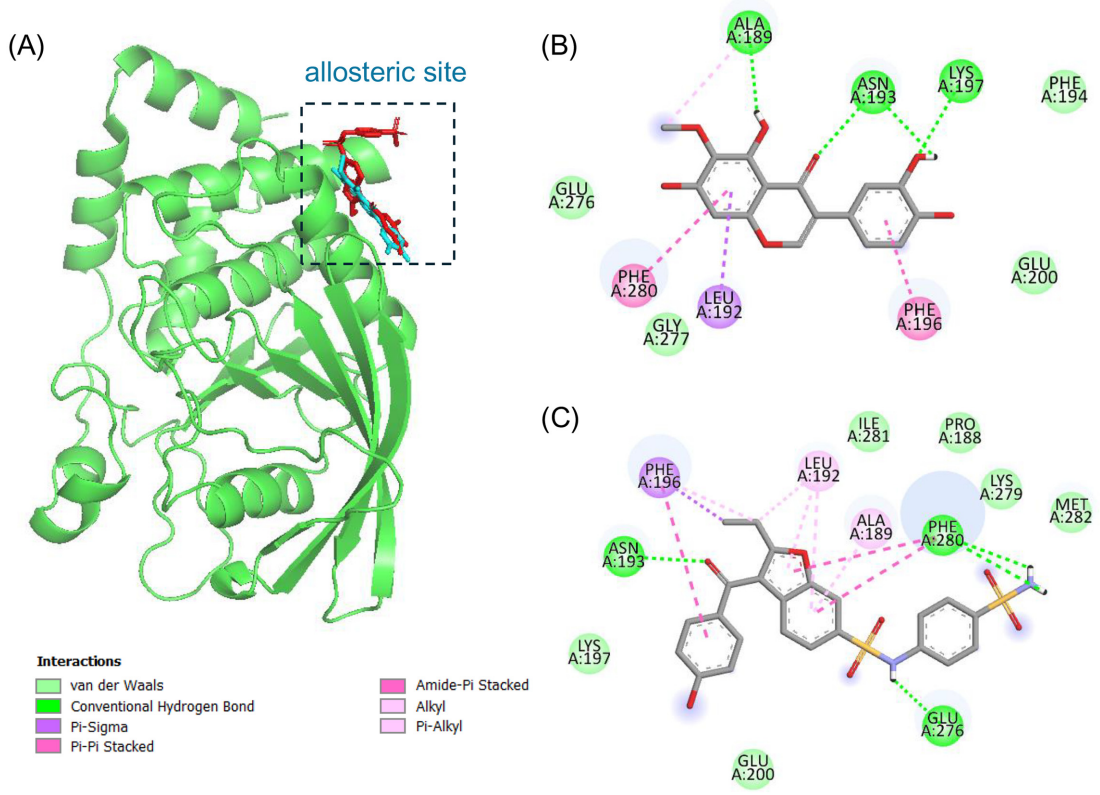

Fig. 3. Molecular docking related PTP1B inhibition by compound A (red stick) and **8** (cyan stick) (A). 2D diagram of PTP1B inhibition by **8** (B) and compound A (C) at the PTP1B allosteric site. The figure was generated using PyMOL and Discovery Studio Visualizer.

With −7.92 kcal/mol of binding energy, the corresponding ligand interactions of irilin D (**8**) at the allosteric site of PTP1B were four hydrogen bonding interactions between its ketone and hydroxyl groups and three interacting residues: Asn193, Ala189, and Lys197. Van der Waals interactions were observed between irilin D (**8**) and PTP1B residues Glu276, Phe194, Glu200, and Gly277, which may help this compound further be stabilized in the active site of PTP1B. In addition, irilin D (**8**) and compound A shared some similar binding residues, including the allosteric residue Asn193 via H-bond interaction; Glu200 via van der Waals interaction; and Phe196, Ala189, Phe280, and Leu192 via hydrophobic interactions. The molecular docking result indicated the good binding ability of irilin D (**8**) to the allosteric site of PTP1B, confirming its noncompetitive type of PTP1B inhibition.

Based on molecular docking studies using AutoDock 4.2 software, binding site-directed inhibition of α-glucosidase by irilin D (**8**) was predicted, in which (*Z*)-3-butylidenephthalide (BIP) was selected as the standard ligand for validating the simulation results. The results are shown in Fig. 4 and Table 3, which include the binding energy, interacting residues with the type of interactions including H-bond, van der Waals, and hydrophobic interactions. The ligand-enzyme complexes of irilin D (**8**)/or BIP were posed stably in the same pocket (allosteric site) of the α-glucosidase enzyme with negative binding energies of −8.23 and −6.86 kcal/mol, respectively. The α-glucosidase-irilin D (**8**) inhibitor complex contained five hydrogen bonds with three interacting residues Cys342, Glu296, and Asn259. In addition, van der Waals interactions with Lys16, Thr340, Asp341, Trp343, Ser298, Thr290, Trp15, Lys13, His295, and Ile272 residues stabilized the α-glucosidase-irilin D (**8**) complex. One hydrophobic interaction (π-σ) was observed between irilin D (**8**) and the Ala292 residue. As listed in Table 3, irilin D (**8**) and BIP shared many similar binding residues including Glu296 via H-bond interaction; Lys16, Asp341, Trp343, Ser298, and Thr290 via van der Waals interactions; and Leu292 via hydrophobic interaction. Taken together, the findings of kinetic analysis and molecular docking simulation showed that the α-glucosidase inhibitory activity of irilin D (**8**) was promising. Interestingly, the α-glucosidase inhibition of irilin D (**8**) *in silico* was recently recognized and reported via its molecular docking simulation with the 3TOP receptor (a part of α-glucosidase enzyme in human gut).[25]

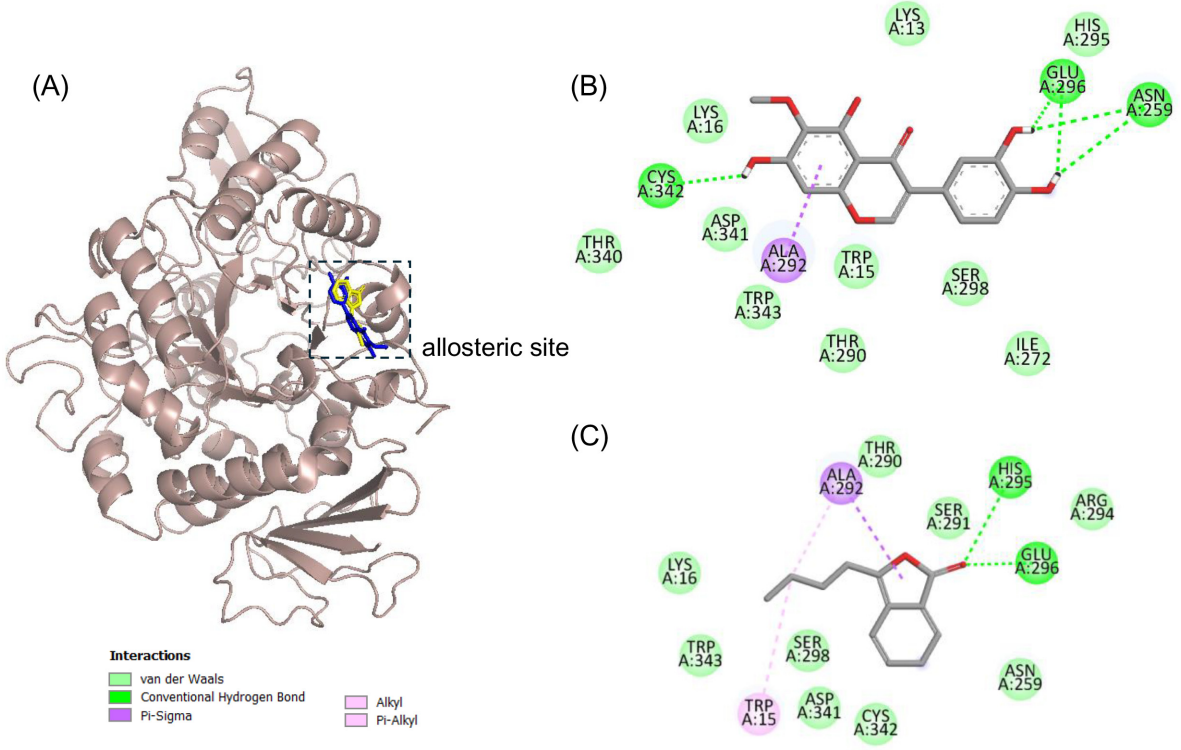

Fig. 4. Molecular docking related α-glucosidase inhibition by BIP (yellow stick) and **8** (blue stick) (a). 2D diagram of α-glucosidase inhibition by **8** (b) and BIP (c) at the allosteric site of α-glucosidase. The figure was generated using PyMOL and Discovery Studio Visualizer.

In conclusion, our present study reports the isolation and investigation of the anti-diabetic activity of sixteen *B. chinensis* compounds (twelve isoflavonoids and four flavonoids) via their inhibitory ability against α-glucosidase and PTP1B enzymes *in vivo* and *in silico*. The results showed that two isoflavonoids (irilin D and genistein) act as dual α-glucosidase and PTP1B inhibitors. The first kinetic investigation of irilin D indicated its noncompetitive inhibition type for both of these two enzymes. In addition, molecular docking simulations of irilin D and the reference ligands showed negative binding energies and similar proximity to residues in the PTP1B and α-glucosidase binding pocket, which means they are closely connected and strongly binding with the active enzyme site. Thereby suggesting the potential of *B. chinensis* isoflavonoids in the prevention and treatment of type-2 diabetes.

Acknowledgments

This research was supported by the National Research Foundation of Korea (NRF) of Korea (NRF-2021R1A 2C2011940) and Gyeongsangbukdo (RISE).

Conflicts of Interest

The authors declare that they have no conflicts of interest.

References

(1) Ogurtsova, K.; Guariguata, L.; Barengo, N. C.; Ruiz, P. L.-D.; Sacre, J. W.; Karuranga, S.; Sun, H.; Boyko, E. J.; Magliano, D. J. *Diabetes Res. Clin. Pract.* **2022**, *183*, 109118.

(2) Mezza, T.; Cinti, F.; Cefalo, C. M. A.; Pontecorvi, A.; Kulkarni, R. N.; Giaccari, A. *Diabetes* **2019**, *68*, 1121–1129.

(3) Ferhati, X.; Matassini, C.; Fabbrini, M. G.; Goti, A.; Morrone, A.; Cardona, F.; Moreno-Vargas, A. J.; Paoli, P. *Bioorg. Chem.* **2019**, *87*, 534–549.

(4) Tamrakar, A. K.; Maurya, C. K.; Rai, A. K. *Expert Opin. Ther. Pat.* **2014**, *24*, 1101–1115.

(5) Ha, M. T.; Lee, T. H.; Kim, C. S.; Prajapati, R.; Kim, J. A.; Choi, J. S., Min, B. S. *Phytochemistry* **2022**, *197*, 113100.

(6) Woźniak D.; Matkowski A. Fitoterapia **2015**, *107*, 1–14.

(7) Li, J.; Ni, G.; Liu, Y.; Mai, Z.; Wang, R.; Yu, D. *J. Nat. Prod.* **2019**, *82*, 1759–1767.

(8) Zhang, L.; Wei, K.; Xu, J.; Yang, D.; Zhang, C.; Wang, Z.; Li, M. *J. Ethnopharmacol.* **2016**, *186*, 1–13.

(9) Liu, M.; Yang, S.; Jin, L.; Hu, D.; Wu, Z.; Yang, S. *Molecules* **2012**, *17*, 6156–6169.

(10) Ha, M. T.; Gal, M.; Kim, J. A.; Lee, J.-H.; Min, B. S. *Bioorg. Chem.* **2024**, *143*, 107066.

(11) Ha M. T.; Le T. T.; Nguyen, V. T.; Kim J. A.; Choi J. S.; Min B. S. *Phytochem. Lett.* **2023**, *57*, 231–238.

(12) Monthakantirat, O.; De-Eknamkul, W.; Umehara, K.; Yoshinaga, Y.; Miyase, T.; Warashina, T.; Noguchi, H. *J. Nat. Prod.* **2005**, *68*, 361–364.

(13) Hanawa, F.; Tahara, S.; Mizutani, J. *Phytochemistry* **1991**, *30*, 157–163.

(14) Al-Khalil, S.; Al-Eisawi, D.; Kato, M.; Iinuma, M. *J. Nat. Prod.* **1994**, *57*, 201–205.

(15) Balza F.; Towers G. H. M. *Phytochemistry* **1984**, *23*, 2333–2337.

(16) Matsumoto T.; Tahara S. *J. Agric. Chem. Soc. Jpn.* **2001**, *75*, 659–667.

(17) Won, S. W.; Woo, E. H. *Phytochemistry* **1993**, *33*, 939–940.

(18) Choudhary, M. I.; Nur-e-Alam, M.; Baig, I.; Akhtar, F.; Khan, A. M.; Ndögnii, P. Ö.; Badarchiin, T.; Purevsuren, G.; Nahar, N.; Atta-ur-Rahman. *J. Nat. Prod.* **2001**, *64*, 857–860.

(19) Qin, M. J.; Ji, W.-L.; Wang, Z.-T.; Ye, W.-C. *J. Integr. Plant Biol.* **2005**, *47*, 1404–1408.

(20) Herz, W.; Sudarsanam, V. *Phytochemistry* **1970**, *9*, 895–896.

(21) Jung, S. H.; Lee, Y. S.; Lee, S.; Lim, S. S.; Kim, Y. S.; Shin, K. H. *Arch. Pharm. Res.* **2002**, *25*, 306–312.

(22) Ito, H.; Onoue, S.; Yoshida, T. *Chem. Pharm. Bull.* **2001**, *49*, 1229–1231.

(23) Seong, S. H.; Roy, A.; Jung, H. A.; Jung, H. J.; Choi, J. S. *J. Ethnopharmacol.* **2016**, *194*, 706–716.

(24) Genovese, M.; Nesi, I.; Caselli, A.; Paoli, P. *Molecules* **2021**, *26*, 4818.

(25) Yehia, S. M.; Ayoub, I. M.; Watanabe, M.; Devkota, H. P.; Singab, A. N. B. *Sci. Rep.* **2023**, *13*, 5233.

Received May 29, 2025
Revised June 18, 2025
Accepted June 19, 2025